The Quadrupole as a Source of Energetic Particles: III. High Speed Solar Wind Streams and MeV electrons

R. B. Sheldon
NASA/MSFC/NSSTC/SP62

T. A. Fritz, Jiasheng Chen, Boston University
Boston University

Abstract

The recent observation that high speed solar wind streams associated with extensions of the solar polar coronal holes during the declining phase of the solar sunspot cycle cause very different magnetospheric response than the more equatorial, interplanetary coronal mass ejections during solar maximum can be understood in terms of the magnetospheric cusp transducer. We begin by applying the trapping properties of the static equinoctal cusp to the problem of the dynamic response to interplanetary transients. Several of the peculiar statistics of energetic particle correlations can be understood as a non-linear, multi-parameter dependence on the solar wind driver. Accordingly, we show data that support this high latitude location as the origin of the outer radiation belt MeV electrons, and the location of the solar wind energy transducer. This identification permits the formulation of more accurate MeV electron predictors, which we think can explain some of the empirical predictors recently published.

1. Introduction

In earlier papers, [*Sheldon et al.*(2005)*Sheldon, Fritz, and Chen*; *Sheldon et al.*(2006)*Sheldon, Fritz, and Chen*,] (SCF1,SCF2), we argued that a quadrupole trap could function as an accelerator, a cross between a dipole and Fermi-accelerator, possessing the best features of both. In SCF2 we presented in more detail the way this physical mechanism may explain the somewhat mysterious origin of outer radiation belt MeV electron (ORBE) injections [*McIlwain*(1996),], and physically link them to solar wind conditions that impact the quadrupole cusp. This placement of source of ORBE outside the dipole

but inside the magnetosphere may account for the relatively recent discovery by POLAR [*Sheldon et al.*(1998)*Sheldon, Spence, Sullivan, Fritz, and Chen*; *Chen et al.*(1997)*Chen, Fritz, Sheldon, Spence, Spjeldvik, Fennell, and Livi*; *Chen et al.*(1998)*Chen, Fritz, Sheldon, Spence, Spjeldvik, Fennell, Livi, Russell, and Gurnett*,]. Likewise, the physical mechanism we propose may also explain some of the peculiar correlations and non-linear relations observed between ORBE injections and solar wind/magnetospheric activity [*Paulikas and Blake*(1979); *Baker et al.*(1986)*Baker, Blake, Klebesadel, and Higbie*; *Koons and Gorney*(1991); *Li et al.*(2001b)*Li, Temerin, Baker, Reeves, and Larson*,].

As we argued in SCF1, a trap is thermodynamically preferred for acceleration, both because the efficiency of energy conversion is higher for a multi-step, stochastic process, and because the total energy required for particle acceleration in minimized. The quiescent, static trap does not accelerate, but in order to understood the dynamics, the ground state of the static trap must be understood. That was the subject of SCF2, which showed the trapping limits of the empty equinoctal cusp was rigidity dependent, and matched both the ring current ion energy range, as well as the ORBE energy range.

In this paper, we show how solar wind transients perturb the Hamiltonian around an assumed equilibrium solution, and can provide the changing conditions favorable to acceleration. Accordingly in section two, we discuss the quasi-static equilibria of the outer cusp, and the conditions required for stable trapping during a transient. In section three we discuss the requirements for stochastic acceleration in the cusp, basing it on the more well-understood Fermi-I,II mechanism, and compare this to several interplanetary disturbances. In section four we show how a high-latitude source is consistent with observations of MeV electron injections, and provides a framework for interpreting the statistical correlations.

2. The Quasi-Static Cusp

2.1. The Equinoctal Cusp

We traced both protons and electrons through a quadrupolar cusp region of a T96 [*Tsyganenko and Stern*(1996),] magnetosphere for 093 Julian date in IGRF epoch year 2000 at 0000 UT, using a solar wind of 3/cc at 400 km/s and +10nT Bz north ($\equiv$Bn). These conditions are known to be favorable for cusp trapping as we show later. Dst is a nominal +10 nT characteristic of an extended quiet period with little or no ring current, but as we demonstrate later, has little effect on the cusp. We calculated the center of the cusp to be at GSE coordinates (6.88, -0.04, 10.1) at a radius of 12.23 Re from the Earth.

Particles were given initial conditions at various perpendicular radii (0-6 Re), and at various parallel distances (-3 to 1 Re) from this central point at two different MLT "sides" of the cusp, 0000 and 1200MLT. The program looped through a range of energies (200-6000 keV) and local pitchangles (70°, 80°, and 90°), or five nested loops altogether. For each starting location, we calculated provisional cusp invariants as follows. The magnetic moment was defined normally, the perpendicular energy divided by magnetic field strength. The gyrophase for all particles was started at 0. The cusp second invariant should be calculated by integrating the parallel velocity along the bounce orbit, instead we used the proxy of the cusp equatorial pitch angle (CEqPA), or the pitchangle of the particle when it arrives at the high latitude minima on the gyrocenter field line. The bounce phase was taken to be the distance from the cusp equator along the fieldline, and was started from -3 Re to +1 Re. Finally, the cusp third invariant should be proportional to the flux enclosed by a drift orbit around the cusp, but without knowing beforehand whether the drift trajectory was closed, we used as a proxy the Euclidean distance from the

fieldline minima to the quadrupole center (C-shell). The drift phase was the clock angle around the cusp (CLT) relative to the quadrupole null rather than the Earth's surface field, with 1200 being in the plane that included the sun and the B-field vector at the quadrupole null.

In terms of these provisional invariants, the calculated trajectories (details in SCF2 [*Glasel et al.*(1999)*Glasel, Sullivan, and Fritz*; *Press et al.*(1986)*Press, Teukolsky, Vetterling, and Flannery*,]) are classified as "trapped" or "chaotic" based on their ability to drift completely around the cusp following "lily-orbits" ([*Sheldon et al.*(1998)*Sheldon, Spence, Sullivan, Fritz, and Chen*,]) where we used the approximation that $\tau > 33$ minutes (about two drift orbits) inside a GSE box ((0,20),(-12,12),(-1,20)) is "trapped", whereas $3 < \tau < 33$ minutes are "quasi-trapped". (The approximation is only problematical for low energy electrons, because particle tracing with inaccurate B-field led to "stalling" of the drifts.) In Figure 1 we plot the thousands of protons and electrons traced through the cusp as trapped (blue), quasi-trapped (red), or chaotic (green) in a four panel projection of the 3-D phase space. In the lower left is a 3-axis projection, whereas the remaining panels show projections into two dimensions only. Note that the axes are arranged so that the three 2-D panels can be folded into the sides of a box.

From the upper left panel for electrons in Fig 1, we see that the maximum magnetic moment cutoff for trapping electrons is about 50 keV/nT, with a cusp equatorial pitchangle (CEqPA) ranging from 45°-90°. The minimum magnetic moment cutoff at 3 keV/nT we attribute to numerical truncation errors in the T96 magnetic field model (discussed in SCF2), which would vanish (permitting all lower magnetic moments to be trapped) if a better numerical field model were used.

The upper right panel shows that the C-shell varies from 1-5 Re, with a high threshold that depends on CEqPA, larger for 90°. The absence of trapping below C-shell$\sim$1 we attribute to the very small $|B|$ near the quadrupole center which destroys the invariants. Note the number of quasi-trapped orbits at large C-shell, which we attribute to the CLT asymmetry of the quadrupole cusp, which is especially shallow at dawn and dusk, so that electrons are trapped for less than a full drift orbit.

Finally, the bottom right panel shows a similar quasi-linear dependence of the high C-shell with magnetic moment, larger for smaller magnetic moment. We recognize the same 3 keV/nT numerical limit seen in the left panel. Reference to the lower left panel, shows that the trapped (blue) points form a compact cloud surrounded by untrapped or quasi-trapped orbits, demonstrating that phase space is well-ordered and analytic, that trapping is truly occurring.

Now if these trapped particles pitchangle scatter, they will not change their energy, but they will change their magnetic moment and simultaneously their 2nd cusp invariant. That is, they will escape the high-latitude minima and travel along the magnetic field line toward the dipole equator. Depending on their CLT, this field line could be on the dayside, around the flanks or down the tail. Alternatively, the cusp could dynamically change its topology due to a solar wind transient, and the 2nd invariant could vanish, leading to the same effect as particle pitchangle scattering. Finally, a transient could betatron energize the particle due to a cusp compression, which may exceed the rigidity-dependent trapping limit in magnetic moment or Cshell. Once again, the escaping particle will appear at the dipole equator, but (by conservation of the first invariant) with much the same magnetic moment as it had in the cusp trap.

2.2. Solar Wind control of Cusp Topology

The MeV electron particle tracing in the equinoctal cusp plot above required thirteen months of CPU time on a 1.8 GHz dual AMD machine. Therefore computational resources limit the number of cases we can run in order to map out the trapping limits under varied solar wind conditions. It is computationally easy, however, to examine the stable cusp trapping volume to show that the most fragile invariant is often the 2nd. That is, the high latitude magnetic minima is often very shallow and strongly dependent on topology. Accordingly we measure the depth of this minima using a T96 magnetic model on a high latitude fieldlines for several solar wind conditions, showing the depth of the minima, $\Delta B_{HI-LAT} = B_{MAX} - B_{MIN}$. This value is then assigned to the footpoint, mapping it to its ionospheric location. Figure 2 shows these high latitude depth mappings for three variables: solar wind pressure, dipole tilt, and Dst, while holding Bn constant, with contours at 1, 3, and 10 nT.

Note that there are two pieces of the high latitude minima, the lower latitude "sausage", and the higher latitude "halo". Between them is the quadrupole null where fieldline tracing becomes numerically noisy. The lower latitude minima result from solar wind compression of the subsolar point, whereas the higher latitude minima result from compression on the poleward side of the cusp. These compressions must be mediated by currents, as illustrated by a popular magnetosphere current diagram [*Kivelson and Russell*(1995),], which shows that the subsolar magnetopause current is dawn-dusk, whereas the poleward cusp current is dusk-dawn, and can be imagined as a Chapman-Ferraro (CF) current "vortex" encircling the cusp in the direction that enhances the subsolar current. This CF vortex current system has the same diamagnetic properties as the ring current, but circulating in the opposite direction from the dipole trapped current. This produces a natural quadrupole with a null magnetic field between the two. It also means that the CF fields are repelled by the ring current, so that increases in dipole |Dst| generate a repulsive force on the cusp, and an expansion of the volume of magnetosphere.

However, the CF vortex and the subsolar current are not a closed system, but parts of a distributed current that can return through the tail or neutral sheet and bypass the cusps altogether. Therefore while coupled, they can change independently. For example, reconnection changes this current system, with Bz southward ($\equiv$Bs) "shorting out" the subsolar current, and Bn affecting the poleward current. Likewise, a tilt of the dipole toward the sun reduces the subsolar current while simultaneously increasing the poleward current.

Figure 2 shows that the poleward minima is much more transient than the subsolar minima, and that for negative dipole tilt away from the sun, the "halo" can even completely vanish. This is very significant, because both minima must be present if the trapped particles traced above are to drift completely around the cusp and possess a cusp 3rd invariant. Thus for some topological configurations of the T96 cusp, there are no cusp trapped particles. We also note that the locations where the 2nd invariant is most likely to fail are in the two dawn or dusk boundary regions between the poleward minima and subsolar minima [*Zong et al.*(2003)*Zong, Fritz, Korth, Daly, Dunlop, Balogh, Reme, and Dandouras*,].

Figures 3 and 4 show that large |Dst| magnifies the ionospheric footpoint without changing its overall shape. If a halo exists, and a 3rd invariant is still possible, |Dst| merely enhances the effect without changing the topology. This might be understood by the diamagnetic effect of the CF vortex, causing the CF currents to scale proportional to the ring current, but without changing the topology.

We also note the significant change caused by solar wind pressure. Higher pressure naturally enhances

the subsolar current, but under certain conditions also causes the magnetosphere to "flare". That is, [*Roelof and Sibeck*(1993),] show that a combination of either Bs and low pressure, or Bn and high pressure cause the sides of magnetosphere to move outward. And a flared magnetopause tilts the cusp sunward, forcing the poleward currents to enhance, which in turn, deepen the poleward minima halo.

Therefore two different types of dynamical configurations can increase the trapping ability of the cusp: a sunward tilt of the dipole, and a high pressure Bn solar wind stream. Conversely, Bs under sufficiently high solar wind pressure will weaken the poleward minima. And Dst has no dynamical effect on the cusp trapping topology, though it may enhance an existing effect.

2.3. Dipole Appearance of the Injection

Mapping electrons at constant magnetic moment from the cusp to the dipole gives a upper limit of 50 keV/nT, which around L=5 Re or 240 nT corresponds to an energy of 12 MeV. That is, the highest energy ORBE map to the magnetic moment upper limit of the cusp trapping region.

Since the $|B|$ minima in the cusp is usually shallower than the corresponding dipole equator, the dipole equatorial pitchangle of the escaping particles varies between 30°-90°, with a probable peak away from 90°. In the outer dipole magnetosphere, or in the tail, the equatorial field strength can often be smaller than that of the $1 < C < 6$ region, which would exclude cusp particles from the near 90° pitchangles. The near 0° pitchangles are also excluded because of the wider "loss cones" of the cusp trapped population. As a consequence, the escaping pitchangle distributions (PAD) will appear as "butterfly" PAD, especially in the outer magnetosphere. Subsequent diffusion into the inner dipole magnetosphere would tend to drive these butterfly PAD toward a 90° peaked or "pancake" PAD, but residues of the butterfly PAD may still be discernible as a dip at 90° [*Horne et al.*(2003)*Horne, Meredith, Thorne, Heynderickx, Iles, and Anderson*,].

Finally the cusp trap does not map to the entire dipole, it only has access to the outer regions of the dipole. The smallest dipole L-shell which threads through the cusp trap occurs at noon, and determines the minimum L-shell boundary for cusp particle "injections" into the dipole. It depends on the topology of the cusp, which varies with UT, but for the equinoctal cusp this minimum L-shell will be at its maximum yearly value. That is, the solstices should have deeper penetration of cusp injections than the equinoxes.

3. Fluctuation Power

Once the cusp possesses a sufficiently deep poleward minima, and a 3rd invariant is possible, then the trap begins to fill and power can injected or extracted from the trap. As discussed in both [*Sheldon et al.*(1998)*Sheldon, Spence, Sullivan, Fritz, and Chen*; *Sheldon et al.*(2005)*Sheldon, Fritz, and Chen*,], and illustrated by Tables 13 and 23, the three resonant frequencies for MeV electrons in the cusp are approximately 0.1s gyration, 0.5s bounce and 20-200s drift.

Whether due to inaccuracies in particle tracing, magnetic field roundoff errors, or actual chaotic behavior of the particles, the particle tracing gave a range of values for the invariants, to which we have assumed a gaussian spread, (rarely the case), and fit a sigma using the steep side of a skewed distribution, which we also tabulate. When a distribution is double valued, we have used the peak with greater number

of events. In all cases, sigma is a minimum estimate, with true distributions having much larger spreads. When no sigma is given, the statistical approach failed, and we estimated the value by another method. When the bounce period is less than 4 times the gyration period, it becomes difficult to separate them, with the most common error being the misidentification of a half-bounce period as a full bounce, though other “half-harmonics” are also possible. The CEqPA was estimated two ways: the initial pitchangle and local B-field were used with the minimum B-field discovered by tracing the field-line to estimate an initial CEqPA, alternatively, the maximum and minimum B-field encountered in the first 65485 timesteps were used to estimate a “global” minimum CEqPA. While the global value might easily be lower, an underestimate of the initial CEqPA might be attributed to uncertainty in tracing the appropriate B-fieldline in the presence of strong gradients.

Table 1. Selected Cusp-Trapped Electron Timescales.

Energy MeV	Gyration τ_1 ms	Bounce τ_2 ms	Drift τ_3 sec	μ keV/nT	CEqPA Deg	Cshell Re	name file
0.2	87+41	186+22	8.08+.44	28.1+1.3	61.2/60.1	0.77	0200_05–05_70
0.2	71+18	1255+475	241	10.08+.16	82.9/77.7	2.42	0200_25–10_90
0.2	44.6+6.3	679+644	328	9.22+.10	80.5/76.5	3.43	0200_40_15_90
0.2	38.1+5.5	697+610	564	7.98+.10	80.2/79.4	4.22	0200_50_00_90
0.2	36.8+7.7	670+590	1130	7.28+.22	80.4/79.7	4.91	0200_60_00_90
0.4	12.1+3.4	305+26	69.0+1.8	18.48+.41	40.1/51.2	1.26	0400_05–15_70
0.4	12.1+3.3	460+24	368	13.99+.14	49.2/55.6	2.12	0400_10–20_90
0.4	22.2+3.4	90+72	13.02+.40	42.4+1.1	82.7/69.9	1.31	0400_15_00_90
0.4	11.7+3.0	215+48	132	20.10+.28	82.9/77.1	2.42	0400_25–10_90
0.4	17.5+4.4	182+40	103	18.32+.37	76.5/74.6	3.54	0400_40_15_90
0.4	11.9+3.2	214+35	176	15.86+.45	80.3/75.3	4.22	0400_50_00_90
0.4	10.1+1.9	288+24	384	14.38+.29	80.4/77.2	4.91	0400_60_00_90
0.6	28.4+7.5	710+200	49+2	25.34+.61	40.1/50.9	1.26	0600_05–15_70
0.6	24.2+5.0	500+140	63.6	30.22+.63	56.4/58.3	1.83	0600_10–15_90
0.6	122+50	400+140	9.1+1.1	62.6+1.7	82.7/65.9	1.31	0600_15_00_90
0.6	112+35	280+100	95.4+1.6	30.27+.61	82.9/73.5	2.42	0600_25–10_90
0.6	75+30	300+24	128	27.60+.36	80.5/74.3	3.43	0600_40_15_90
0.6	58+13	360+20	221	23.94+.50	80.3/74.5	4.22	0600_50_00_90
0.6	91+32	310+90	333	21.78+.74	80.4/74.9	4.91	0600_60_00_90
0.8	34.5+7.0	342+90	37.6+3.3	37.3+1.1	40.1/50.9	1.26	0800_05–15_70
0.8	34.2+6.8	630+140	70.5+1.1	35.29+.52	51.5/56.0	1.83	0800_10–15_70
0.8	112+43	185+62	6.0+1.2	85.2+4.3	82.8/62.3	1.31	0800_15_00_90
0.8	37.3+8.7	65+20	74.5+1.5	40.04+.54	82.9/73.9	2.42	0800_25–10_90
0.8	30.4+9.4	64+19	101.2+1.3	36.48+.84	80.5/73.6	3.43	0800_40_15_90
0.8	28.1+6.7	231+58	173	32.0+1.1	80.3/74.8	4.22	0800_50_00_90
0.8	29.9+7.8	430+96	326	28.82+.87	80.4/74.6	4.91	0800_60_00_90
1.0	38+12	545+59	32.2+1.6	47.1+1.9	40.1/45.5	1.26	1000_05–15_70
1.0	46+16	567+59	57.4+1	44.4+1.3	51.5/55.2	1.83	1000_10–15_70
1.0	76+23	259+52	11.8+1.5	81.9+5.9	68.0/60.3	1.35	1000_15–05_70
1.0	75+22	435+49	63.4+1.9	49.8+1.3	82.9/69.4	2.42	1000_25–10_90
1.0	65+15	229+42	85.3+2.0	45.6+1.2	80.5/71.3	3.43	1000_40_00_90
1.0	53+18	275+30	143.6+.5	39.6+1.0	80.3/74.2	4.22	1000_50_00_90
1.0	53+16	115+32	218.5+1	35.95+.95	80.3/74.3	4.91	1000_60_00_90

Table 2. Selected Cusp-Trapped Electron Timescales.

Energy MeV	Gyration τ_1 ms	Bounce τ_2 ms	Drift τ_3 sec	μ keV/nT	CEqPA Deg	Cshell Re	name file
1.2	50+15	580+68	26.0+4.3	55.7+5.0	42.4/49.8	1.26	1200_05–15_80
1.2	50+14	557+86	50.0+1.4	53.0+1.7	51.5/55.2	1.83	1200_10–15_70
1.2	245+75	381+56	22.0+1.2	78.6+1.4	81.2/70.9	2.00	1200_15–10_90
1.2	105+36	222+43	53.6+1.6	59.81+.69	82.9/72.1	2.42	1200_25–10_90
1.2	136+25	536+95	73.4+1.8	54.1+1.4	80.5/70.7	3.43	1200_40_00_90
1.2	128+39	644+110	123.5+1.2	47.13+.82	80.3/73.9	4.22	1200_50_00_90
1.2	105+38	406+54	187.5+1.2	42.93+.75	80.4/74.0	4.91	1200_60_00_90
1.4	82+22	599+68	44.6+1.7	60.8+2.2	51.5/54.2	1.83	1400_10–15_70
1.4	95+25	321+36	19.0+1.5	92.8+2.7	81.2/69.1	2.00	1400_15–10_90
1.4	91+24	280+45	48.0+2.1	69.6+2.2	82.9/66.9	2.42	1400_25–10_90
1.4	86+22	306+48	63.0+1.4	64.+1.1	80.5/74.2	3.43	1400_40_00_90
1.4	47+12	586+32	105.4+2.0	55.5+1.0	80.3/74.1	4.22	1400_50_00_90
1.4	48+13	630+230	165.	50.13+.96	80.4/73.6	4.91	1400_60_00_90
1.6	93+32	560+100	39.6+2.1	71.0+3.1	51.5/55.1	1.83	1600_10–15_70
1.6	204+85	323+75	18.0+1.4	102.5+6.4	81.2/62.1	2.00	1600_15–10_90
1.6	184+80	416+63	41.2+1.0	79.7+2.0	82.9/71.8	2.42	1600_25–10_90
1.6	327+66	368+37	57.3+1.7	71.9+2.2	80.5/68.9	3.43	1600_40_00_90
1.6	215+53	653+49	99.8+1.1	62.1+1.6	79.6/72.0	4.13	1600_50_00_90
1.6	357+40	831+62	147.33+.83	57.2+1.6	79.7/72.6	4.82	1600_60_00_90
2.0	151+50	725+130	45.7+2.0	79.5+5.0	52.1/52.2	2.03	2000_11–16_70
2.0	122+42	646+84	62.9+1.7	79.8+3.1	60.0/60.8	2.53	2000_16–16_70
2.0	126+43	304+70	65.0+1.6	81.9+2.4	75.8/67.6	2.97	2000_21–16_90
2.0	171+52	319+77	86.3+1.8	77.1+1.7	83.5/72.6	3.28	2000_26–16_90
2.0	177+27	347+48	119.90+.91	71.45+.58	90.0/76.5	3.41	2000_31–16_90
2.0	154+37	310+31	176.31+.79	67.00+.47	84.2/77.7	3.56	2000_36–16_90
3.0	280+178	607+114	28.1+2.0	133.+15.	52.1/53.7	2.03	3000_11–16_70
3.0	295+96	815+360	47.8+2.0	114.7+9.4	60.0/57.2	2.83	3000_16–16_70
3.0	244+67	532+190	41.9+1.7	126.1+3.6	75.9/65.1	2.97	3000_21–16_90
3.0	289+92	563+131	60.0+2.1	115.5+2.5	83.5/68.5	3.28	3000_26–16_90
3.0	191+36	398+87	119.7+.70	107.2+.88	90.0/76.5	3.41	3000_31–16_90
3.0	279+61	579+106	123.1+1.1	100.10+.79	84.2/76.0	3.56	3000_36–16_90
4.0	468+139	832+294	48.0+1.1	149.6+7.5	65.7/58.1	2.97	4000_21–16_70
4.0	525+174	814+162	52.8+1.0	148.1+6.8	78.1/62.5	3.28	4000_26–16_80
4.0	456+128	894+191	64.0+2.1	143.4+3.6	90.0/68.7	3.40	4000_31–16_90
4.0	375+112	875+124	95.7+1.4	133.3+1.8	84.1/73.5	3.56	4000_36–16_90
6.0	499+144	1105+277	53.0+2.3	206.5+5.0	71.6/62.8	4.61	6000_31–21_90
6.0	644+227	1324+251	65.8+1.4	198.7+2.0	84.1/72.4	3.56	6000_36–16_90
6.0	494+136	1017+308	68.2+1.7	198.2+4.3	82.9/70.8	5.76	6000_46–21_90

Therefore fluctuations in cusp topology or magnetic field in the frequency band between 6mHz-20Hz

can couple power to these electrons. In SCF1 we discuss synchronous or resonant fluctuations, in which the disturbance is always going the same direction each time the particle returns to its approximately initial condition. For example, if the cusp were always shrinking, say, by a continually increasing solar wind pressure, then betatron acceleration would energize the particles in the same direction. This has been modeled by [*Delcourt et al.*(2005)*Delcourt, Malova, Zelenyi, Sauvaud, Moore, and Fok*,] showing significant acceleration. Or if the cusp were always shrinking whenever the particles were at local noon, but expanding at local midnight, then the third drift invariant would be resonant with the cusp disturbance.

The other kind of acceleration discussed in SCF1 is stochastic or non-resonant. In this type of acceleration the cusp compression can occur at all phases and times, so that the population of trapped particles has an equal likelihood of gaining energy as losing. This type of acceleration is diffusive in energy-space, and other things being equal, is less efficient than resonant acceleration. However, it is also more probable, so that the net power can far exceed the resonant mechanism. In terms of the one-dimensional compressive trap found at the bowshock, which accelerates in the $E_{||}$ direction, these two mechanisms are called Fermi-I and Fermi-II [*Fermi*(1949),]. In our application to the quadrupole trap, the compression is two-dimensional, accelerating in the $E_{\perp}$ direction, and following SCF1 we call it Alfvén-I and Alfvén-II acceleration.

Now the cusp topology responds to both internal and external transients, so that, for example, substorm tail stretching also flares the magnetopause enhancing cusp trapping, whereas substorm dipolarizations detrap so that the 20 minute substorm timescale may couple to the cusp drift resonance through small changes in B. The waves generated by substorms, however, are likely to tranmit more power than these low frequency topology changes, since higher frequency Alfvénic fluctuations should have more Poynting flux, as [*Hassam*(1995),] has argued, since the cusp is a low-Q absorber for Alfvén waves.

But in terms of sheer power, the internal sources pale in comparison to the solar wind driver. Operating over an area of several square Re on the dayside magnetopause, a sudden fluctuation in solar wind pressure or density changes the CF currents as it pushes the magnetopause in or out. When we consider that the CF currents are immediately adjacent to the cusp and encircle it, then we begin to see that increases in the CF vortex which, say, are responding to a 10% increase in solar wind pressure, cause far more than a 10% energy increase in the cusp trap. Because the magnetopause shrinks in a self-scaling way for certain pressure and Bn regimes [*Roelof and Sibeck*(1993),], a 10% ($\sim$1 Re) reduction in the subsolar distance would result in a 27% reduction in volume of the cusp trap, magnifying the solar wind fluctuation. Accordingly the cusp trap is an especially sensitive transducer for converting solar wind mechanical energy into fluctuation power for accelerating particles.

Of course, solar wind fluctuation power of the correct resonant frequency will also rapidly accelerate the trapped population. But such peaks in the solar wind fluctuation spectral density are not observed, instead a broad maximum centered near 2mHz indicates that solar wind is structured on a roughly 30 Re spatial scale. Therefore non-resonant processes are more likely to accelerate the trapped particles. In addition, the fluctuations within cusp diamagnetic cavities approach $\Delta B/B \sim 1$, [*Chen and Fritz*(1998),], while the relative proximity (0.1s/0.5s/100s) of the adiabatic resonances permit diffusion of the invariants, both necessary ingredients for stochastic acceleration.

Note that this transducer is insensitive to solar wind electrical power. That is, the rectified solar wind electric field, Ey=Vx·Bs, causes the magnetopause to trim (not flare), which detraps the cusps. This effectively distinguishes the cusp transducer from the tail transducer, or the mechanical from the electri-

cal response of the magnetosphere. Note also that it is energetic electrons that are trapped in the cusp, not cold electrons, because the existence of the third invariant, like the ring current ions, depends on energetic, ∇B-drift overcoming the $E \times B$-detrapping. Accordingly, this transducer cannot be modelled by MHD, and does not correspond to either Poynting flux or Joule heating. Finally note that our discussion of trapped flux, both in SCF1 and SCF2 has used the statistically generated T96 or T01 models of the magnetospheric cusp, and has not taken into account the observed diamagnetic cavities from POLAR [*Chen and Fritz*(2001); *Chen et al.*(2001)*Chen, Fritz, Sheldon, Pickett, and Russell*; *Chen and Fritz*(2002),], which provide feedback from particles trapped in the cusp and change the trap topology.

4. MeV Electron Injections

Having developed a rough outline of the dynamic behavior of trapped electrons in the cusp, we can now apply it to the four decades of data and statistics for the Earth's outer radiation belts. Our goal in this section is to find an explanation for heretofore unexplained ORBE correlations, and make predictions that can be tested by future experiments.

4.1. Prototypical Injection Profile

Recent papers [*Friedel et al.*(2002)*Friedel, Reeves, and Obara*; *Dmitriev and Chao*(2003); *Vassiliadis et al.*(2005)*Vassiliadis, Fung, and Klimas*,] trace the history of the ORBE problem that has been recognized since the 1960's. ORBE peak in flux intensity around L$\sim$4, with fluxes rising rapidly over a time span of about 2-3 days, and over an Lshell range $3 < L < 8$. The outer range is approximate, because there is no dipole 3rd invariant at large distances ([*Roederer*(1970),]), and because dynamic effects such as magnetopause motion can remove these particles. Later studies [*Selesnick and Blake*(2000); *Hilmer et al.*(2000)*Hilmer, Ginet, and Cayton*; *Onsager et al.*(2004)*Onsager, Chan, Fei, Elkington, Green, and Singer*,] show that when expressed as phase space density (PSD), the ORBE injections usually show a constant or radially increasing PSD from geosynchronous outward, suggesting an outer boundary source transported rapidly inward. This is consistent with a diffusion rate that varies as $D_{LL} \propto L^{6+}$. However, the data sets are not conclusive, with some arguing for a transient inner magnetosphere peak in PSD, suggesting an internal source [*Green and Kivelson*(2004),].

The origin of these MeV electrons is neither in the solar wind, in the tail, in the magnetosheath, nor on flux tubes connected to Jupiter's MeV electron population. Although isolated events, such as the March 1991 solar wind shock are effective at locally accelerating MeV electrons, the typical MeV event is uncorrelated with shocks. Statistical correlations of ORBE injections were found to be poorly correlated ($R < 0.6$) with internal magnetospheric indices: Dst, AE, Kp; as well as poorly correlated with solar wind parameters: Ey, Akasofu ϵ, B_Z, ρ, ρV^2. The best correlation is V_{SW}, [*Paulikas and Blake*(1979),], which could produce a linear regression coefficient $R \sim$0.8, but only in a one to two year time span on the declining phase of the solar cycle. [*Li et al.*(2001b)*Li, Temerin, Baker, Reeves, and Larson*,] have pursued these statistics, and with an empirical diffusion model, have managed to achieve $R \sim$0.9 linear correlation coefficients for a one-year span around 1996.

[*Ballatore*(2002),] using advanced statistical techniques found a solar wind speed threshold of 550 km/s necessary for ORBE effects. [*O'Brien et al.*(2001)*O'Brien, McPherron, Sornette, Reeves, Friedel, and Singer*,] used superposed epoch analysis of Dst minimum, which reached the same conclusions:

high speed wind is the most important variable. They argue, however, for an internal source of energy in Pc5 ULF as a secondary correlator. [*Vassiliadis et al.*(2005)*Vassiliadis, Fung, and Klimas*,] refines this approach, using finite impulse response (FIR) filters keyed to the solar wind velocity to carry out a more extensive search for correlations, which when binned by L-shell, show that the greatest correlator depends on L-shell.

All these statistics show correlation, but causation remains undetermined. In contrast, we formulate a causal relationship between "recurrent magnetic storms" due to high speed solar wind and ORBE injections via cusp trapping.

4.2. High Speed Solar Wind Triple Play

As we have established in section 2, the high latitude cusp trap responds very differently to solar wind pressure transients depending on the direction of B_Z, with low-pressure Bs slightly enhancing the trap, but high pressure Bn being the clear winner. Therefore the ICME solar wind transients that cause the largest geoeffective, Dst magnetospheric response, those that have Ey, are often the ones with the weakest MeV production and vice versa [*Ballatore*(2002); *Ballatore*(2003),]. With sufficiently large driving, whether Ey or pressure, this clear separation breaks down and many other acceleration pathways are energetically allowed, so that superstorms generate plenty of everything. Therefore this anti-correlation between Dst storms and ORBE injections is most noticeable for weak and moderate storms, as we have suggested before [*Sheldon and Spence*(1998),], but now we present a model to explain the correlation.

There are more characteristics of high speed solar wind, however, that amplify the ORBE effectiveness of these transients. As the Ulysses mission ably demonstrated, high speed solar wind comes from the solar polar corona, and it is also thought that reconnection in this region generate magnetic fieldline "kinks" that produce the high Alfvénic turbulence of this type solar wind. The combination of high speed, high pressure, and high turbulence is a triple play for the cusp dynamics.

4.2.1. High Pressure. First, the high pressure with Bn, give us the flared magnetopause and the enhanced poleward B-field minima. This creates the preconditions of a cusp 3rd invariant necessary for a cusp trap to form, as we discussed earlier. But in addition, Bn also enhances the stability of a cusp 3rd invariant. Since the cusp trap only functions for energetic particles that can ∇B-drift around the quadrupole minima, the presence of an electric potential across the cusp will prevent cold plasma from completing a drift orbit. So a 5 kV change across the cusp becomes a $\sim$5 keV energy threshold for trapping, depending on the topology. Since this is above the 0.1 keV peak in the solar wind electron distribution, one would not expect too many magnetosheath electrons to become trapped.

Note that increasing solar wind Ey, or Bs, increases the electric field across the cusp, which raises the energy threshold, making geoeffective ICME's with strong Ey less likely to cause trapping in the cusp. Alternatively, it is conceivable for Bn to reconnect above the cusp, creating counter-potentials that lower the energy threshold, making Bn more ORBE-effective. Finally, we note that electrons are ubiquitous, and even if solar wind electrons are too cold to be trapped, this does not preclude magnetospheric electrons from collecting in the trap, or suprathermal solar wind electrons found in the non-thermal, powerlaw tails. To demonstrate that high speed solar wind and/or solar wind Ey can abruptly and non-linearly "switch on" the trapping of thermal electrons, we calculate the number of electrons above the "trapping threshold" energy.

4.2.2. Kinetic Temperature. This is the second way that high speed solar wind improves the trap, since the average kinetic energy is higher so that as the solar wind thermalizes in the magnetosheath, the average temperature of the particles is higher. Since the fast and slow solar wind interact as they leave the sun, with the fast wind "overexpanding" as it comes out of the coronal hole, the density of the fast wind is less than that of the slow wind and must be corrected for the calculation below. Using an average density of slow wind at 10.3/cc, fast wind at 3.4/cc, with average speeds of 330 km/s and 700km/s, [*Holzer*(1992),] the density of the fast wind is found to be inversely proportional to velocity, $n \propto 1/v^{\gamma}$ with a rough index $\gamma = 1.44$.

Then the number of particles above some velocity threshold for a Maxwellian thermal distribution is (cf. [*Abramowitz and Stegun*(1964),] formula 7.1.22),

$$F(x,\beta) = n\beta^3 \int_x^{\infty} v^2 e^{-\beta^2 v^2} dv = n(0.25\sqrt{\pi}[1 - \mathrm{erf}(\beta x)] + 0.5x\beta e^{-\beta^2 x^2}) \quad (1)$$

where erf is the error function, $x \equiv \sqrt{2E/m}$ is the threshold velocity, $\beta \equiv \sqrt{1/2kT}$ is the isotropic temperature, and n is the normalization to the average density. If we define the ratio of temperatures for fast to slow solar wind as, $\alpha \equiv \sqrt{T_f/T_s}$, then $\beta_f = \alpha\beta_s$. Finally, the relative increase in the number of particles $v > x$ as a function of α and $x\beta$ for fixed energy threshold becomes,

$$P(\alpha, x\beta) \equiv (F_f/\alpha^{\gamma} - F_s)/F_s \quad (2)$$

where we use α as a proxy for solar wind speed. We tabulate P as a function of α and $E/kT(= 2x^2\beta^2)$ in Table 34.2.2.

Table 3. Relative Flux Increase for Fast Over Slow Wind

E/kT	1.5	3	6	12	24	48	72
α							
5.00	-0.856	-0.751	-.143	11.3	3.19e3	2.67e8	2.14e13
4.00	-0.802	-0.660	0.151	14.8	3.70e3	2.45e8	1.53e13
3.00	-0.704	-0.499	0.623	19.1	3.66e3	1.41e8	5.01e12
2.00	-0.489	-0.189	1.253	18.5	1.64e3	1.25e7	8.59e10
1.50	-0.280	0.027	1.228	10.3	3.04e2	2.31e5	1.55e08
1.25	-0.138	0.091	0.815	4.22	4.35e1	3.26e3	2.13e05
1.10	-0.050	0.066	0.366	1.28	5.40e0	4.97e1	3.65e02

Note the negative entries that occur when the energy threshold is too low, and the decrease in the peak density of the fast solar wind more than outweighs the increase in the tail, resulting in a net reduction. Also note that when calculating the relative increase, we divided by the slow solar wind F_s, which may approach zero and result in unphysically large relative increases. One should view these unphysical numbers as simply binary, saturated at "on" or "off". Therefore the transmitted flux is a non-linear function of threshold energy, switching on over a relatively short interval around $E/kT \sim 10 - 20$.

If typical slow solar wind electron temperatures in the sheath are 0.1 keV, then doubly fast (800km/s) solar wind should be somewhere between 0.3-0.4 keV in temperature, depending on polytropic index

in the sheath. Data from POLAR/TIDE [*Elliott et al.*(2001)*Elliott, Comfort, Craven, Chandler, and Moore*,] suggest that the perpendicular velocity for cold hydrogen in the outer cusp region is about 10km/s, corresponding to 1.2kV/Re electric fields, if all the perpendicular velocity is driven by electric fields rather than, say, gradient drifts. The particle tracing discussed earlier suggests that typical drift paths around the cusp might be as small as 1 Re diameter, though POLAR found diamagnetic cavities up to 6 Re in diameter [*Fritz et al.*(2003)*Fritz, Chen, and Siscoe*; *Chen et al.*(2005a)*Chen, Fritz, and Sheldon*,]. This gives a range of 1.2 - 7.2 kV for potentials across the cusp, which determines the threshold energy. Then the E/kT parameter is about 12–72 with $\alpha \sim 2$. From Table 34.2.2, this gives a relative increase $P(E/kT, \alpha) = [(12, 2), (72, 2)] = [(18.5), (9e10)]$, or from partially open to wide open.

Since the radius of the drift orbit determines the magnitude of E/kT, and the radius is determined primarily by C-shell, which is roughly the distance from the quadrupole null as projected on the magnetopause, then the number of particles that might diffuse across the magnetopause at a given E/kT, is proportional to the annular area, $N \propto A = \pi(\mathrm{Csh}_2^2 - \mathrm{Csh}_1^2) \propto E/kT$. By inspection of Table 3, this further steepens the non-linear relative increase for fast wind, by weighting the higher threshold particles.

Finally, if diamagnetic cavities form in the cusp (CDC), as observed by [*Chen et al.*(1998)*Chen, Fritz, Sheldon, Spence, Spjeldvik, Fennell, Livi, Russell, and Gurnett*; *Chen and Fritz*(1998); *Chen and Fritz*(2000); *Chen et al.*(2001)*Chen, Fritz, Sheldon, Pickett, and Russell*; *Chen and Fritz*(2002),], then the mapping along magnetic field lines from the magnetopause goes around the quadrupole null (now spread out over the CDC) totally excluding drift orbits from the interior of the CDC (since the gradient of B is zero in this region). Then transmitted magnetosheath electrons are forced to arrive some distance away from the quadrupole null, with a minimum E/kT cutoff energy. A future paper will discuss the topology changes due to CDC, but here we merely note its amplifying effect on this non-linear switch.

This may explain then, the non-linear change in correlation coefficients when the fast solar wind exceeds 550 km/s noted by [*Ballatore*(2002),]. From the table, this corresponds to an $\alpha \sim 1.5$, with a threshold at $E/kT \sim 12$. For a 0.1 keV slow solar wind temperature scaled to $T_f = \alpha^2 T_s = 0.25keV \rightarrow 3kV$, which from a POLAR/TIDE electric field of 1.2 kV/Re, would correspond to 2.5 Re diameter, or a drift C-shell of about 1.2 Re. While we were not able to trace electrons at this low an energy due to truncation errors in the B-field model, Table 1&2 shows that this Cshell was near the lower limit for stable trapping of 200-1200 keV electrons, and presumably stable for 3 keV electrons as well.

4.2.3. Alfvénic Turbulence. The third base in this triple play is the enhanced Alfvénic turbulence of the high speed solar wind. This turbulence not only preheats the electrons (increasing α without decreasing n), but more importantly, it appears at the magnetopause as fluctuations in total pressure. And the location where the magnetopause is "softest", like a worn shock absorber, is the cusp. Therefore solar wind turbulence induces large $\Delta B/B$ changes in the cusp, and causes large transverse heating $\mathrm{E}_\perp$ [*Chen and Fritz*(1998),]. We have argued above and in SCF1 that stochastic heating, or Alfvén-II acceleration delivers the most power to the trapped particles, so we expect the rise in the energy of the trapped electrons to follow a diffusion timescale, with higher energies requiring a longer time. (Of course, the energy diffusion coefficient depends on the fluctuation power available, so that all energies will rise faster when there is higher turbulence.) If one characterizes the seed energy spectrum as a power law, then this time dependent energization appears as a convex break in the power law spectrum that moves toward higher energy with time.

If our analysis is correct, that Dst makes no change in the cusp topology or trapping, then our model predicts that Dst should have no correlation with MeV electrons. However, many such correlations have been published, which we discuss in the next section.

4.3. Dst versus MeV storms

There has been some confusion concerning the relation between Dst and ORBE injections. Early work [*Nagai*(1988); *Koons and Gorney*(1991),], showed that Dst was a poor predictor of ORBE, and that of the internal indices, Kp showed the most promise. However, [*Reeves*(1998),] showed what appeared to be nearly a 100% correlation between the occurrence of Dst storms and appearance of MeV electrons, though he later showed [*Reeves et al.*(2003)*Reeves, McAdams, Friedel, and O'Brien*,] a much smaller correlation with magnitude. Therefore recent studies, such as [*O'Brien et al.*(2001)*O'Brien, McPherron, Sornette, Reeves, Friedel, and Singer*,], argue that the Dst always precedes the MeV injection, and is a necessary, though not sufficient, condition for ORBE injection, such that we must identify what other necessary elements are missing. [*Li et al.*(2001a)*Li, Baker, Kanekal, Looper, and Temerin*,] plot SAMPEX data of MeV electrons versus L-shell and overplot Dst purporting to show a quantitative relation between the magnitude of Dst and the depth of penetration and magnitude of MeV electrons. How can these later correlations be consistent with the earlier lack of correlation?

We think it can be explained by separating the Dst response into two components: 1) solar wind Ey, and 2) solar wind σ_P (dynamic pressure variations). The Dst is a magnetic disturbance roughly caused by trapped keV ions in the ring current about 3 Re from the Earth [*Dessler and Parker*(1959); *Sckopke*(1966),]. This can change for two reasons: a) the ring current is carrying more amperes because ions are injected; or, b) the ring current is closer to the Earth. Solar wind Ey tends to do both, injecting ions from the tail through enhanced convection, and pushing the duskside closer to the earth. Note that a linear electric field tends to shift the ring current off center, without necessarily shrinking the radius, which to first order, should change the magnetic disturbance D_{ASYM}, not the D_{SYM} that contributes to the Dst. Incomplete longitudinal coverage of magnetic stations, as well as magnetospheric complexities such as field-aligned currents can make these asymmetric currents appear in the Dst. Nevertheless, the major impact of Ey is the injection of convecting plasmasheet ions into the ring current, which occurs over a 1-2 hour period.

In contrast, higher fluctuation power in the solar wind leads to enhanced diffusive transport [*Schulz and Lanzerotti*(1974),]. The inner edge of the ring current, marked by a sharp decrease in ion density ([*Sheldon and Hamilton*(1993); *Sheldon*(1994a),], occurs as result of the equilibrium between the ion transport from large L and the loss from charge exchange with atmospheric neutrals. When the transport coefficients increase, the inner edge equilibrium moves Earthward, and |Dst| increases [*Sandanger et al.*(2005)*Sandanger, Soraas, Aarsnes, Oksavik, Evans, and Greer*,]. One characteristic of this type of |Dst| injection is a 6-12 hour ragged or gradual increase in |Dst|, with none of the abruptness or magnitude of Ey injections. It is only when Dst is averaged over a day or more ([*Reeves*(1998); *Li et al.*(2001a)*Li, Baker, Kanekal, Looper, and Temerin*,]), that the two types of Dst injections appear qualitatively similar.

Now we have said that high speed solar wind streams are especially effective at forming the cusp trap, and trapping electrons. Since high speed wind typically has a large fluctuation power, which enhances radial diffusion, it is often correlated with the 2nd type of Dst injection. This is especially true

in [*Reeves*(1998),] study, or in the oft-quoted 1995-1996 correlation year. High speed wind associated with Bs, will perhaps have an effect on both Dst and ORBE, whereas other sources of solar wind Ey will have negligible effect on ORBE. This can be seen in the superposed epoch analysis of [*O'Brien et al.*(2001)*O'Brien, McPherron, Sornette, Reeves, Friedel, and Singer*,], where a high density solar wind that produces |Dst| is anti-correlated to MeV injections, and likewise, strong Bs that rotates northward, or strong |B| in general are somewhat anti-correlated.

Finally, the high correlation of Dst with inner edge of the radiation belts observed by [*Li et al.*(2001a)*Li, Baker, Kanekal, Looper, and Temerin*,] can be a consequence of increased transport, not necessarily injection. Likewise the apparent correlation of Dst with MeV electron flux can also be a consequence of increased transport without injection, since as PSD moves Earthward, the adiabatic energization applied to a falling powerlaw spectrum appears as increased flux. Like Dst, then, the two sources of increased flux can be either transport or injection, but these plots do not separate the two.

Therefore the earlier study of geosynchronous PSD (taking out the adiabatic effects on fluxes), which depend on MeV injection rather than transport are correct in not finding a strong Dst correlation, since Dst is a consequence of either Ey or inner magnetospheric transport. However, the intriguing model of [*Li et al.*(2001b)*Li, Temerin, Baker, Reeves, and Larson*,] argues that at least during 1996, a diffusive transport code modulated by solar wind conditions can achieve R$\sim$0.9 in predicting MeV electron fluxes at GEO, suggesting no MeV injection is needed, only an outer magnetospheric transport mechanism.

The major difference between this GEO result using solar wind-driven transport and the SAMPEX inner L-shell result of [*Li et al.*(2001a)*Li, Baker, Kanekal, Looper, and Temerin*,] using Dst-driven transport, is that transport outside geosynchronous remains somewhat speculative, since SAMPEX, even with 90 minute L-shell scans, does not observe dynamic MeV electron motion at these L-shells. Nor is there sufficient satellite coverage to get unequivocal simultaneous measurements of MeV electrons at multiple L-shells outside GEO. Furthermore, the [*Li et al.*(2001b)*Li, Temerin, Baker, Reeves, and Larson*,] calculation of a 2-3 day diffusive transport rate is not consistent with $\sim$1 day storm diffusion timescales [*Schulz and Lanzerotti*(1974),], or SAMPEX daily plots, which show a much faster transport rate. In order to achieve a more observationally consistent 2-3 day transport timescale, then, would require smaller diffusion coefficients and larger radial flux gradients with a large flux at the distant boundary. [*Taylor et al.*(2004)*Taylor, Friedel, Reeves, Dunlop, Fritz, Daly, and Balogh*,] used the CLUSTER instrumentation to look for these putative large PSD sources and found only 1% of what was predicted. This suggests that if transport is occurring, it has a smaller gradient, and a necessarily larger diffusion coefficient than expected. Therefore Li's model with constant MeV electron source at L=11 and transport-limited access to geosynchronous is probably a simplification of the more general model with a time-variable source, which would permit the 2-3 day timescale to be located in the boundary condition rather than the transport rate, such as in the simulation of [*Spjeldvik and Fritz*(1981),].

4.4. Kp/AE versus MeV indices

Other magnetospheric indices have been examined for ORBE prediction, including Kp and AE. [*O'Brien et al.*(2001)*O'Brien, McPherron, Sornette, Reeves, Friedel, and Singer*,] argue for the presence of ULF Pc5 in the Dst recovery phase, as well as an elevated AE in the recovery phase as indicative of MeV particle enhancements. [*Vassiliadis et al.*(2005)*Vassiliadis, Fung, and Klimas*,] show that AE only becomes a better predictor than V_{SW} or Kp for L-shells outside geosynchronous. If this is the re-

gion of ULF acceleration, it suggests an outer magnetosphere source, possibly consistent with Li's outer boundary condition. Of course, AE is measured in the auroral zone, so perhaps it is not surprising it correlates well in this region. If it were the sole source, however, it should correlate to inner regions of the magnetosphere, what [*Vassiliadis et al.*(2005)*Vassiliadis, Fung, and Klimas*,] refer to as a "coherent" response, which was not found.

This lack of L-shell coherence might be due to the SAMPEX observations of particle flux in a spectral "window", which would map to different parts of the PSD distribution. That is, diffusive transport connects high energy flux at L=3 with low energy flux at L=7, which should behave coherently if transport is great enough. If, however, the flux SAMPEX observes at $L > 7$ correspond to energies higher than the SAMPEX/PET energy threshold at L=4, it cannot see this coherence. Then it is possible that AE might really be responsible for injecting particles at L=8, but SAMPEX cannot record these particles at L=4, hence the lack of AE correlation there.

Arguing that the SAMPEX measurements have an L-shell dependent coherence length, makes the conclusion that each L-shell has different solar wind or internal drivers ([*Vassiliadis et al.*(2005)*Vassiliadis, Fung, and Klimas*,]) not surprising. Note that solar wind Ey, which we relate to their Bs set of indices, is an external driver, and has difficulty penetrating into the inner magnetosphere. Accordingly, it can produce $\sim$100 keV particles with a strong polar cap electric field, but as these tail electrons convect toward the earth, they divert around the inner magnetosphere. The last closed drift path for various electric field configurations, the Alfvén layer, separates these energized tail particles from trapped magnetosphere particles, which for this energy range lies just inside geosynchronous orbit (lower energy ring current ions penetrate further, perhaps to L=4 [*Sheldon*(1994b),]). Inside this L-shell, transport is diffusive, requiring violation of the 3rd invariant. Therefore it is also not surprising that above L=6 we see Ey factors being the best correlators, and below L=6 we see diffusive terms, related to V_{SW}, becoming dominant.

At about L$<$4, [*Vassiliadis et al.*(2005)*Vassiliadis, Fung, and Klimas*,] find a completely different response, one that is not coherent with the $4 < L < 7$ response. This population responds almost immediately to an increase in solar wind speed without the usual 2-3 day delay, and is well correlated with Kp. This correlation is often called the "Dst effect" [*Li et al.*(1997),], whereby the ring current abruptly and adiabatically changes the topology of the inner magnetosphere. Outside the ring current the magnetic field intensity increases, whereas inside the ring current the intensity decreases. Now the drift orbit of an energetic particle roughly conserves the encircled polar magnetic flux, so that if the field strength goes up, its orbit (mapped to the pole) must shrink, and the particle moves toward higher L-shells [*Sheldon and Gaffey*(1993),]. This explains the anti-correlation observed at large L-shells, because as the particles move toward higher L, they also adiabatically de-energize. And the conservation of particles would suggest that increasing the volume should decrease the flux.

However, inside the ring current, the field decreases, which forces the particles to move the other direction, inward. This adiabatically increases the particle energy, and by compressing the volume, increases the flux [*Kim et al.*(2001)*Kim, Rostoker, and Kamide*,]. Now the fast, positive correlation of this region with Ey becomes clear: it is the same Dst effect driven by ring current observed a lower L-shells, which is primarily Ey-driven.

Since the purpose of this paper is to correlate MeV fluxes with injections, we will ignore the fast, $\sim$1 day adiabatic shifting of the PSD due to transport, and focus only on the effects that have a 2-3 day risetime and require an injection of MeV electrons. To distinguish between the two effects, we look

for characteristics unique to injection. Two key signatures that are relatively unaffected by transport are spectra and pitchangle. Both spectra and pitchangles show the effect of adiabatic energization, as $E_\perp$ increases with increasing B-field, but subsequent transport does not change the spectral index or remove features from the pitchangle distribution (PAD). This makes spectral and pitchangle information critical in discerning injection mechanisms.

4.5. Pitchangle Distribution of Injections

The asymmetries of the Earth's dipole field, primarily caused by the solar wind compression and tail current stretching, cause energetic particles with differing pitchangles to drift on non-overlapping orbits [*Roederer*(1970),]. This drift shell splitting of MeV electrons, which causes a radial gradient in the flux to map to a "butterfly" distribution at midnight, and a "pancake" distribution at noon, is well-known [*West et al.*(1973)*West, Buck, and Walton*,] and has been most recently observed and discussed by [*Selesnick and Blake*(2002),] using the POLAR data set. However, comparison of model simulations and observations, show that the model, even when initialized with observed data at a single MLT, consistently overpredicts the drift shell splitting actually observed. This overprediction only gets worse with higher Kp as the magnetosphere is compressed by solar wind, as during a high speed stream. The most common explanation given–pitchangle scattering is isotropizing the distribution–would also increase the loss rate, which is not observed. Therefore [*Selesnick and Blake*(2002),] suggest that "This may show that the source location of the relativistic electrons, that is the location where they are accelerated, is distributed in local time."

We draw two other conclusions from this paper, that quiet times, without any additional MeV injections, show the strongest drift shell splitting effects, precisely because the distributed source has been turned off. Therefore when large butterfly or pancake distributions are observed, we can either infer that we are observing a quiescent magnetosphere (readily determined from the Kp history), or the peculiarities of the source injection directly. But we cannot conclude that stormtime injections have a fixed pitchangle distribution at a single local time that subsequently evolves to explain all butterfly distributions observed.

This then leads to the observations of peculiar pitchangles during a MeV storm injection by [*Horne et al.*(2003)*Horne, Meredith, Thorne, Heynderickx, Iles, and Anderson*,]. Butterfly distributions are observed for some orbits L>4, E>1MeV, and for all orbits that passed through the equator at large L-shell. They may have been present on all orbits, but higher latitude CRRES orbits cannot observe the near-equatorial pitchangle minima, whose exclusion results in a "flat-topped" distribution. Whereas wave-particle acceleration can achieve flat-topped PADs, apparently they do not produce butterfly PADs unless the acceleration occurred as "a result of nonlocal acceleration occurring at higher (lower) latitudes." Furthermore, were wave-particle acceleration the explanation, it would have to occur for higher energies only, since "Inspection of higher resolution data at 0.1L ... shows that there is a pancake at 214 keV and a butterfly distribution at 1.47 MeV all the way between L = 5.05–6.05. Data averaging to achieve a spatial resolution of 0.1L takes approximately 3 min at L = 4 and 6 min at L = 6. However, it takes the spacecraft more than 1 hour to move between these two locations. Thus we conclude that the energy dependence in the butterfly distributions is not due to time of flight effects."

As we argued above, high-latitude acceleration in the cusps meet all the criteria of the observations: an accelerated population off the equator to generate butterfly distributions, a distributed MLT source so

as to minimize the drift-shell splitting, and a high-energy, E>1 MeV source. Next we discuss additional data supporting the spectral break around 1 MeV.

4.6. Spectral Breaks

In general, magnetospheric electron populations have a high energy powerlaw tail above some thermal peak [*Christon et al.*(1989)*Christon, Williams, Mitchell, Frank, and Huang*; *Christon et al.*(1991)*Christon, Williams, Mitchell, Huang, and Frank*,], the "kappa" distribution, also named for mathematician Mittag-Leffler a century earlier. Therefore a spectral index is often sufficient to describe the high energy part of the spectra, and is assumed when calculating the average energy of detector bin [*Contos*(1997),], in a "bow-tie" analysis [*Selesnick and Blake*(2000),]. This spectral index is affected differently by different acceleration mechanisms, and therefore can provide an important discriminator between mechanisms.

Consider the transport of MeV electrons into the inner magnetosphere through radial diffusion that violates the third invariant but conserves the first. Since $\mu = E_\perp/|B|$ is conserved, then as $|B|$ increases, so must the perpendicular energy. The amount of energization is proportional to $f = B_f/B_i$, the ratio of the final to initial $|B|$. Since a powerlaw spectrum is a straight line in log-log space, multiplying a spectrum by the factor f results in a constant shift of the entire spectrum toward higher energy, without changing the spectral index at all [*Meredith et al.*(2002)*Meredith, Horne, Summers, Thorne, Iles, Heynderickx, and Anderson*; *Chen et al.*(2005b)*Chen, Fritz, and Sheldon*,].

As a second example, consider a constant electric field applied to a region that is inside the tail. All the particles experience a $\Delta \mathrm{E_i}$ electric field that increases the energy by an amount $E = q\Delta \mathrm{E_i}$. In a log-log energy spectrum, this additive term increases the low energy greatly, but has little effect at high energy, thereby steepening (softening) the powerlaw spectrum, and decreasing the negative index further. Only those particles lower in energy than the thermal peak of the kappa function, only those particles below the powerlaw tail would show a "harder" spectral index, which is opposite to what is generally observed.

Another promising candidate acceleration is betatron acceleration by dB/dt for electrons inside the substorm current loop. Since the gain in energy is proportional to area enclosed by the gyroorbit(s), higher energy electrons gain proportionally more energy. Ignoring the magnetic gradients, the gyro-radius is $\rho = mv/qB$, so the area, $A \propto 2mE/q^2B^2$. The time for a gyro-orbit, $t \propto 2\pi\rho/v \sim k$, so all energies to first order complete the same number of gyroorbits. Thus betatron acceleration increases the energy by a multiplicative constant, $E_f = E_i[1 + 2m/(q^2B^2)]$. When the gyro-radius is larger than the substorm current loop, the energy gain becomes a constant no longer proportional to the area of the gyroorbit, but long before these GeV energies are reached, the electron has drifted through this dipolarization region. In either case, a constant limiting energy is reached, so that a log-log energy spectrum has a break point and the spectral index softens above but remains constant below that breakpoint. That is, this mechanism should produce a peak in the spectrum, roughly at the energy where the drift time across the wedge is equal to the dipolarization time.

A general rule of thumb then, is that an acceleration that "hardens" a spectral index generally occurs below a convex spectral break, or peak in the spectrum, and an acceleration that "softens" or doesn't change at all occurs above such a break. (Concave spectral breaks, such as the cosmic ray "ankle", would behave oppositely.) Therefore careful attention to spectral breaks and indices can provide helpful information on the acceleration mechanism.

Many of the MeV electron instruments use shielded solid state detectors that measure integral flux above some energy threshold [*Baker et al.*(1997),], so that we have only a two or three point spectral approximation. With these coarse measures, [*Bühler et al.*(1998)*Bühler, Johnstone, Desorgher, Zehnder, Daly, and Adams*; *Li et al.*(1999); *Meredith et al.*(2002)*Meredith, Horne, Summers, Thorne, Iles, Heynderickx, and Anderson,*] show that after the main phase of a Dst storm, the MeV spectral index hardens. This suggests that pure radial diffusion, such as the [*Li et al.*(2001b)*Li, Temerin, Baker, Reeves, and Larson*; *Elkington et al.*(1999)*Elkington, Hudson, and Chan,*] model, cannot fully account for the acceleration. And any electric field mechanism invoked would have to move the (thermal) peak in the electrons above the 1-2 MeV energy so that hardening of the spectrum could occur below the peak. Adiabatically mapping the 2 MeV geosynchronous data to the tail injection boundary at $L \sim 8$, gives an electric field of $\sim$1 MV, much greater than that observed. Likewise the substorm induction effect, even when coupled with radial diffusion, would not be expected by our simplistic analysis to harden the spectral index at all. Of course, more complex betatron acceleration, such as [*Ingraham et al.*(1999)*Ingraham, Belian, Cayton, Meier, and Reeves*; *Kim et al.*(2000)*Kim, Chan, Wolf, and Birn,*], which also violate the first and second invariants might harden the spectra, just as wave-particle acceleration can harden the index, but only if the resonance energy peak in the spectrum occurs above our hardened spectra. And finding a candidate wave resonance above 3 MeV is a major challenge to theory.

Table 4. Storm Hardness Ratios

Year.DOY	$>$1.5 MeV rad/day	$>$3.5 MeV rad/day	h
1996.090	2.3	55	4
1996.120	5	110	5
1996.270	4	80	5
1997.010	2	50	3
1998.130	2	80	2.5
1998.240	12	200	6
1999.050	2	60	3
1999.250	3	70	4
1999.290	3	60	5

The integral type instruments also show that the amount of "hardening", the ratio of the highest energy channel to the lower channels, will vary from storm to storm but stay constant within a storm. From [*Baker et al.*(1997); *Kanekal et al.*(2001)*Kanekal, Baker, and Blake,*] (and private communication, Blake 1997), we calculate the hardness ratio of a 60° inclined elliptical satellite "HEO", using the top two integral channels, $E > 1.5, 3.5$ MeV. Table 44.6 summarizes the results. That is, over the 2-3 day risetime of the MeV fluxes, the hardness ratio, h, rises to a a constant value, $h = h_0(1 - e^{kt})$ [*Bühler et al.*(1998)*Bühler, Johnstone, Desorgher, Zehnder, Daly, and Adams,*], which is unique to each storm, and roughly proportional to the "size". This temporal "coherence" suggests a single mechanism operating for the duration of the acceleration time. If it were a resonant acceleration mechanism, we would explain the change in hardness ratio as a energy change of the resonant peak. Accordingly, we

should look for the inflection point in the spectra above our energy range, preferably with a higher energy resolution instrument.

The CRRES satellite had excellent spectral data, but we have only been able to estimate a spectral break $E_B > 1.6$ MeV from published data [*Meredith et al.*(2002)*Meredith, Horne, Summers, Thorne, Iles, Heynderickx, and Anderson*,]. POLAR/HIST [*Blake et al.*(1995),] had the spectral resolution, though not an equatorial satellite. Making the assumption that peculiar PAD distributions do not change the spectral breaks, we can use the POLAR data to search for spectral changes. [*Selesnick et al.*(1997)*Selesnick, Blake, Kolasinski, and Fritz*,] show a quiescent state of the magnetosphere in early 1996, where we find the 1996.120 injection with a spectral break $\sim$ 4.4 MeV at 4.5 L. [*Selesnick and Blake*(1997),] investigated more dynamic periods in the latter half of 1996 having spectral breaks around $\sim$3.4 MeV at $\sim$6 L. The 1997.010 storm received a great deal of attention, and [*Selesnick and Blake*(1998),] showed a spectral break of $\sim$2.7 MeV at 6 L. It is very suggestive that the hardness ratio from integral HEO measurements, and the spectral breaks from POLAR/HIST show similar trends, increasing with storm "size".

If we attribute this spectral break to a whistler mode chorus MeV electron acceleration mechanism such as [*Meredith et al.*(2002)*Meredith, Horne, Summers, Thorne, Iles, Heynderickx, and Anderson*; *Horne et al.*(2005)*Horne, Thorne, Glauert, Albert, Meredith, and Anderson*,], then it corresponds to chorus generating electrons in the 30 keV range. Whereas the 1997 - 1999 storms had significant Dst, the largest MeV event of 1996, the DOY 110 storm, had no discernible Dst event, and therefore, an unlikely candidate for chorus heating. However, it was the largest high speed solar wind event of the year, when two coronal holes that had been pulsing the magnetosphere every 12 days joined together. The conditions for cusp trapping were ideal for this event, suggesting that the spectral breaks observed are a characteristic of the rigidity cutoffs in the cusp trap.

In a later paper, we argue that the storm of 1997.010 was quite unusual, being an abnormally small Ey-driven MeV storm that produced copious amounts of spectrally soft MeV electro flux, which we attribute to a fortuitous combination of winter solstice, diurnal tilt, and solar wind density, that promoted cusp feedback. But for recurrent storms driven by high-speed V_{SW}, we believe that cusp trapping gives the most probable explanation for the observations.

5. Conclusions

In this paper, we have continued our earlier work on the static trapping properties of the cusp, to show how these energy and pitchangle limits map to the dipole trap through dynamic transport. We also attempt to show how high speed solar wind streams are particularly effective at trapping and energizing electrons in the cusp trap. The peculiar characteristics of this trapped population when it is suddenly transported to the dipole leave a unique fingerprint in the energy spectrum, pitchangle and statistical correlations. We compare these predictions with ORBE injections and find that there are remarkable similarities between the predicted and observed ORBE injections. In particular, this high latitude source resolves many puzzling aspects of the injections, including a distant L¿8 yet magnetospheric source, a distributed MLT injection, a strongly butterfly PAD, two high energy spectral breaks that bracket the injection, a correlation to V_{SW} rather than Ey or other energy-derived indices, a 2-3 day risetime, and the lack of a Dst correlation. In a later paper, we discuss the cusp feedback mechanisms that may explain

the correlation of MeV injections with strong, Ey-driven storms, but in this paper we presented only the properties of the cusp energetic electron trap, and its energy coupling to high speed solar wind, the cause of “recurrent” storms.

Acknowledgments. We acknowlege fruitful conversations with colleagues at NASA/MSFC/NSSTC and NASA grants NAG-5 2578, NAG-5 7677, and NAG-5 1197 at Boston University. Figures 2-4 were the work of UAH masters student, Ravi Kinera, and Table 3 in large part to Emmanuel Krivorutsky.

References

Abramowitz, M., and I. Stegun (1964), *Handbook of Mathematical Functions with Formulas, Graphs, and Mathematical Tables*, vol. National Bureau of Standards Applied Mathematics Series 55, U.S. Government Printing Office, Washington, DC.

Baker, D. N., J. B. Blake, R. W. Klebesadel, and P. R. Higbie (1986), Highly relativistic electrons in the earth’s outer magnetosphere 1. lifetimes and temporal history 1979–1984, *J. Geophys. Res.*, *91*, 4265–4276.

Baker, D. N., et al. (1997), Recurrent geomagnetic storms and relativistic electron enhancements in the outer magnetosphere: ISTP coordinated measurements, *J. Geophys. Res.*, *102*, 14,141–14,148.

Ballatore, P. (2002), Effects of fast and slow solar wind on the correlations between interplanetary medium and geomagnetic activity, *J. Geophys. Res.*, *107*(A9, 1227), doi:10.1029/2001JA000144.

Ballatore, P. (2003), Reply to Comment on “Effects of fast and slow solar wind on the correlations between interplanetary medium and geomagnetic activity” by C. B. Wang and J. K. Chao, *J. Geophys. Res.*, *108*(A10, 1387), doi:10.1029/2003JA009840.

Blake, J. B., et al. (1995), CEPPAD: Comprehensive energetic particle and pitch angle distribution experiment on POLAR, in *The Global Geospace Mission*, edited by C. T. Russell, pp. 531–562, Kluwer Academic Publishers.

Bühler, P., A. Johnstone, L. Desorgher, A. Zehnder, E. Daly, and L. Adams (1998), The outer radiation belt during the 10 January, 1997 CME event, *Geophys. Res. Lett.*, *25*(15), 2983–2986.

Chen, J., and T. A. Fritz (1998), Correlation of cusp mev helium with turbulent ulf power spectra and its implications, *Geophys. Res. Lett.*, *25*, 4113–4116.

Chen, J., and T. A. Fritz (2000), Origins of energetic ions in cep events and their implications, *Int. J. Geomagn. Aeron.*, *2*, 31.

Chen, J., and T. A. Fritz (2001), Energetic oxygen ions of ionospheric origin observed in the cusp, *Geophys. Res. Lett.*, *28*(8), 1459–1462.

Chen, J., and T. A. Fritz (2002), The global significance of the cep events, in *Solar-Terrestrial Magnetic Activity and Space Environment*, vol. Cospar Colloq. Ser 14, edited by H. N. Wang and R. L. Xu, pp. 239–249.

Chen, J., T. A. Fritz, R. B. Sheldon, H. E. Spence, W. N. Spjeldvik, J. F. Fennell, and S. Livi (1997), A new temporarily confined population in the polar cap, *Geophys. Res. Lett.*, *24*, 1447–1450.

Chen, J., T. A. Fritz, R. B. Sheldon, H. E. Spence, W. N. Spjeldvik, J. F. Fennell, S. Livi, C. Russell, and D. Gurnett (1998), Cusp energetic particle events: Implications for a major acceleration region of the magnetosphere, *J. Geophys. Res.*, *103*, 69–78.

Chen, J., T. A. Fritz, R. B. Sheldon, J. S. Pickett, and C. T. Russell (2001), The discovery of a new acceleration and possible trapping region of the magnetosphere, *Adv. Space Res.*, *27*(8), 1417–1422.

Chen, J., T. A. Fritz, and R. B. Sheldon (2005a), Multiple spacecraft observations of energetic ions during a high solar wind pressure event, *J. Geophys. Res.*, *110*(A12212), doi:10.1029/2005JA011043.

Chen, J., T. A. Fritz, and R. B. Sheldon (2005b), Comparison of energetic ions in cusp and outer radiation belt, *J. Geophys. Res.*, *110*(A12219), doi:10.1029/2004JA010718.

Christon, S. P., D. J. Williams, D. G. Mitchell, L. A. Frank, and C. Y. Huang (1989), Spectral characteristics of plasma sheet ion and electron populations during undisturbed geomagnetic conditions, *J. Geophys. Res.*, *94*, 13,409–13,424.

Christon, S. P., D. J. Williams, D. G. Mitchell, C. Y. Huang, and L. A. Frank (1991), Spectral characteristics of plasma sheet ion and electron populations during disturbed geomagnetic conditions, *J. Geophys. Res.*, *96*, 1–22.

Contos, A. R. (1997), Complete description and characterization of the high sensitivity telescope (hist) onboard the polar satellite, Master's thesis, Boston University, Boston, MA.

Delcourt, D. C., H. V. Malova, L. M. Zelenyi, J.-A. Sauvaud, T. E. Moore, and M.-C. Fok (2005), Energetic particle injections into the outer cusp during compression events, *Earth Planets Space*, *57*(2), 125–130.

Dessler, A. J., and E. N. Parker (1959), Hydromagnetic theory of geomagnetic storms, *J. Geophys. Res.*, *64*, 2239.

Dmitriev, A. V., and J. K. Chao (2003), Dependence of geosynchronous relativistic electron enhancements on geomagnetic parameters, *J. Geophys. Res.*, *108*(A11, 1388), doi:10.1029/2002JA009664.

Elkington, S. R., M. K. Hudson, and A. A. Chan (1999), Acceleration of relativistic electrons via drift-resonant interaction with toroidal-mode pc-5 ulf oscillations, *Geophys. Res. Lett.*, *26*, 3273–3276.

Elliott, H. A., R. H. Comfort, P. D. Craven, M. O. Chandler, and T. E. Moore (2001), Solar wind influence on the oxygen content of ion outflow in the high-altitude polar cap during solar minimum conditions, *J. Geophys. Res.*, *106*(A4), 6067–6084.

Fermi, E. (1949), *Phys. Rev.*, *75*, 1169.

Friedel, R. H., G. D. Reeves, and T. Obara (2002), Relativistic electron dynamics in the inner magnetosphere–a review, *J. Atm. Solar-Terrestrial Phys.*, *64*, 265–282.

Fritz, T. A., J. Chen, and G. L. Siscoe (2003), Energetic ions, large diamagnetic cavities, and Chapman-Ferraro cusp, *J. Geophys. Res.*, *108*(A1), doi:10.1029/2002JA009476.

Glasel, J., J. D. Sullivan, and T. A. Fritz (1999), *EOS Trans. Suppl*, *SM32D-10*, S283.

Green, J. C., and M. G. Kivelson (2004), Relativistic electrons in the outer radiation belt: Differentiating between acceleration mechanisms, *J. Geophys. Res.*, *109*(A03213), doi:10.1029/2003JA010153.

Hassam, A. B. (1995), Dynamics and dissipation of compressional alfven waves near magnetic nulls, *Phys. Plasmas*, *2*(12), 4662–4664.

Hilmer, R., G. P. Ginet, and T. E. Cayton (2000), Enhancement of equatorial energetic electron fluxes near L = 4.2 as a result of high-speed solar wind streams, *J. Geophys. Res.*, *105*, 23,311 23,322.

Holzer, T. E. (1992), Interplanetary medium, solar wind, in *The Astronomy and Astrophysics Encyclopedia*, edited by S. P. Maran, pp. 336–338, Cambridge University Press, Cambridge.

Horne, R. B., N. P. Meredith, R. M. Thorne, D. Heynderickx, R. H. A. Iles, and R. R. Anderson (2003), Evolution of energetic electron pitch angle distributions during storm time electron acceleration to megaelectronvolt energies, *J. Geophys. Res.*, *108*(A1, 1016), doi:10.1029/2001JA009165.

Horne, R. B., R. M. Thorne, S. A. Glauert, J. M. Albert, N. P. Meredith, and R. R. Anderson (2005), Timescale for radiation belt electron acceleration by whistler mode chorus waves, *J. Geophys. Res.*, *110*(A03225), doi: 10.1029/2004JA010811.

Ingraham, J., R. D. Belian, T. E. Cayton, M. M. Meier, and G. D. Reeves (1999), March 24, 1991, geomagnetic storm: Could substorms be contributing to relativistic electron flux buildup at geosychronous altitude?, *Eos Supplement*, *80*, S294.

Kanekal, S. G., D. N. Baker, and J. B. Blake (2001), Multisatellite measurements of relativistic electrons: Global coherence, *J. Geophys. Res.*, *106*(A12), 29,721–29,732.

Kim, H.-J., A. A. Chan, R. A. Wolf, and J. Birn (2000), Can substorms produce relativistic outer belt electrons?, *J. Geophys. Res.*, *105*, 7721.

Kim, H.-J., G. Rostoker, and Y. Kamide (2001), Radial dependence of relativistic electron fluxes for storm main phase development, *J. Geophys. Res.*, *107*(A11, 1378), doi:10.1029/2001JA007513.

Kivelson, M. G., and C. T. Russell (1995), *Introduction to Space Physics*, New York: Cambridge University Press.

Koons, H. C., and D. J. Gorney (1991), A neural network model of the relativistic electron flux at geosynchronous orbit, *J. Geophys. Res.*, *96*, 5549–5556.

Li, X., D. N. Baker, S. G. Kanekal, M. Looper, and M. Temerin (2001a), Long term measurements of radiation belts by sampex and their variations, *Geophys. Res. Lett.*, *28*(20), 3827–3830.

Li, X., M. Temerin, D. N. Baker, G. D. Reeves, and D. Larson (2001b), Quantitative prediction of radiation belt electrons at geostationary orbit based on solar wind measurements, *Geophys. Res. Lett.*, *28*(9), 1887–1890.

Li, X., et al. (1997), Multisatellite observations of the outer zone electron variation during the november 3–4, 1993, magnetic storm, *J. Geophys. Res.*, *102*(A7), 14,123–14,140.

Li, X., et al. (1999), Rapid enhancements of relativistic electrons deep in the magnetosphere during the May 15, 1997, magnetic storm, *J. Geophys. Res.*, *104*(A3), 4467–4476.

McIlwain, C. E. (1996), Processes acting upon outer zone electrons, in *Radiation Belts Models and Standards*, edited by J. F. L. et. al, AGU, Washington DC.

Meredith, N. P., R. B. Horne, D. Summers, R. M. Thorne, R. H. A. Iles, D. Heynderickx, and R. R. Anderson (2002), Evidence for acceleration of outer zone electrons to relativistic energies by whistler mode chorus, *Ann. Geophys.*, *20*, 967–979.

Nagai, T. (1988), "space weather forecast": Prediction of relativistic electron intensity at synchronous orbit, *Geophys. Res. Lett.*, *15*, 425–428.

O'Brien, T. P., R. L. McPherron, D. Sornette, G. D. Reeves, R. Friedel, and H. J. Singer (2001), Which magnetic storms produce relativistic electrons at geosynchronous orbit?, *J. Geophys. Res.*, *106*(A8), 15,533–15,544.

Onsager, T. G., A. A. Chan, Y. Fei, S. R. Elkington, J. C. Green, and H. J. Singer (2004), The radial gradient of relativistic electrons at geosynchronous orbit, *J. Geophys. Res.*, *109*(A05221), doi:10.1029/2003JA010368.

Paulikas, G. A., and J. B. Blake (1979), Effects of the solar wind on magnetospheric dynamics: Energetic electrons at geosynchronous orbit, in *Quantitative Modelling of Magnetospheric Processes*, *Geophys. Monogr. Ser.*, vol. 21, edited by W. P. Olson, p. 180, AGU, Washington, D.C.

Press, W. H., S. A. Teukolsky, W. T. Vetterling, and B. P. Flannery (1986), *Numerical Recipes: The art of scientific computing*, Cambridge Univ. Press, Cambridge.

Reeves, G. D. (1998), Relativistic electrons and magnetic storms: 1992-1995, *Geophys. Res. Lett.*, *25*, 1817–1820.

Reeves, G. D., K. L. McAdams, R. H. W. Friedel, and T. P. O'Brien (2003), Acceleration and loss of relativistic electrons during geomagnetic storms, *Geophys. Res. Lett.*, *30*, 36–1, doi:10.1029/2002GL016513.

Roederer, J. G. (1970), *Dynamics of Geomagnetically Trapped Radiation*, Springer, New York.

Roelof, E., and D. G. Sibeck (1993), Magnetopause shape as a bivariate function of interplanetary magnetic field b_z and solar wind dynamic pressure, *J. Geophys. Res.*, *98*(A12), 21,421–21,450.

Sandanger, M. I., F. Soraas, K. Aarsnes, K. Oksavik, D. S. Evans, and M. S. Greer (2005), Proton injections into the ring current associated with b_z variations during HILDCAA events, in *Physics and Modeling of the Inner Magnetosphere*, vol. AGU Monograph, helsinki Chapman conf 2003.

Schulz, M., and L. J. Lanzerotti (1974), *Particle Diffusion in the Radiation Belts*, Springer-Verlag, New York.

Sckopke, N. (1966), A general relation between the energy of trapped particles and the disturbance field near the earth, *J. Geophys. Res.*, *71*, 3125.

Selesnick, R. S., and J. B. Blake (1997), Dynamics of the outer radiation belt, *Geophys. Res. Lett.*, *24*(11), 1347–1350.

Selesnick, R. S., and J. B. Blake (1998), Radiation belt electron observations following the january 1997 magnetic cloud event, *Geophys. Res. Lett.*, *25*(14), 2553–2556.

Selesnick, R. S., and J. B. Blake (2000), On the source location of radiation belt relativistic electrons, *J. Geophys. Res.*, *105*, 2607 2624.

Selesnick, R. S., and J. B. Blake (2002), Relativistic electron drift shell splitting, *J. Geophys. Res.*, *107*(A9, 1265), doi::10.1029/2001JA009179.

Selesnick, R. S., J. B. Blake, W. A. Kolasinski, and T. A. Fritz (1997), A quiescent state of 3 to 8 mev radiation belt electrons, *Geophys. Res. Lett.*, *24*(12), 1343–1346.

Sheldon, R. B. (1994a), Ion transport and loss in the earth's quiet ring current 2. diffusion and magnetosphere-ionosphere coupling, *J. Geophys. Res.*, *99*, 5705–5720.

Sheldon, R. B. (1994b), Plasmasheet convection into the inner magnetosphere during quiet conditions, in *Solar Terrestrial Energy Program: COSPAR Colloquia Series*, vol. 5, edited by D. N. Baker, pp. 313–318, Pergamom Press, New York.

Sheldon, R. B., and J. D. Gaffey, Jr (1993), Particle tracing in the magnetosphere: New algorithms and results, *Geophys. Res. Lett.*, *20*, 767–770.

Sheldon, R. B., and D. C. Hamilton (1993), Ion transport and loss in the earth's quiet ring current 1. data and standard model, *J. Geophys. Res.*, *98*, 13,491–13,508.

Sheldon, R. B., and H. E. Spence (1998), A new magnetic storm model, in *Geospace Mass and Energy Flow: Results from the International Solar-Terrestrial Physics Program*, edited by J. Horwitz, pp. 349–354, AGU, Washington, D.C.

Sheldon, R. B., H. E. Spence, J. D. Sullivan, T. A. Fritz, and J. Chen (1998), The discovery of trapped energetic electrons in the outer cusp, *Geophys. Res. Lett.*, *25*, 1825–1828.

Sheldon, R. B., T. A. Fritz, and J. Chen (2005), The quadrupole as a source of energetic particles: I. general considerations, in *Particle Acceleration in Astrophysical Plasmas: Geospace and beyond*, vol. AGU Monograph 156, edited by D. Gallagher, J. Horwitz, J. Perez, R. Preece, and J. Quenby, pp. 197–204.

Sheldon, R. B., T. A. Fritz, and J. Chen (2006), The quadrupole as a source of energetic particles: Ii. the static equinoctal cusp, presented at Huntsville Workshop 2004.

Spjeldvik, W. N., and T. A. Fritz (1981), Observations of energetic helium ions in the earth's radiation belts during a sequence of geomagnetic storms, *J. Geophys. Res.*, *86*, 2317.

Taylor, M. G. G. T., R. H. W. Friedel, G. D. Reeves, M. W. Dunlop, T. A. Fritz, P. W. Daly, and A. Balogh (2004), Multisatellite measurements of electron phase space density gradients in the earths inner and outer magnetosphere, *J. Geophys. Res.*, *109*(A05220), doi:10.1029/2003JA010294.

Tsyganenko, N. A., and D. P. Stern (1996), Modeling the global magnetic field of the large-scale Birkeland current systems, *J. Geophys. Res.*, *101*, 27,187–27,198.

Vassiliadis, D., S. F. Fung, and A. J. Klimas (2005), Solar, interplanetary, and magnetospheric parameters for the radiation belt energetic electron flux, *J. Geophys. Res.*, *110*(A04201), doi:10.1029/2004JA010443.

West, H. I., Jr, R. M. Buck, and R. J. Walton (1973), Electron pitch angle distributions throughout the magnetosphere as observed by OGO 5, *J. Geophys. Res.*, *78*, 1064.

Zong, Q., T. Fritz, A. Korth, P. Daly, M. Dunlop, A. Balogh, H. Reme, and J. Dandouras (2003), A field line topology tracer – cluster energetic electrons observations in the high latitude boundary / cusp regions, *AGU Fall Meeting Abstracts*, pp. A1195+.

320 Sparkman Dr, Huntsville, AL 35805

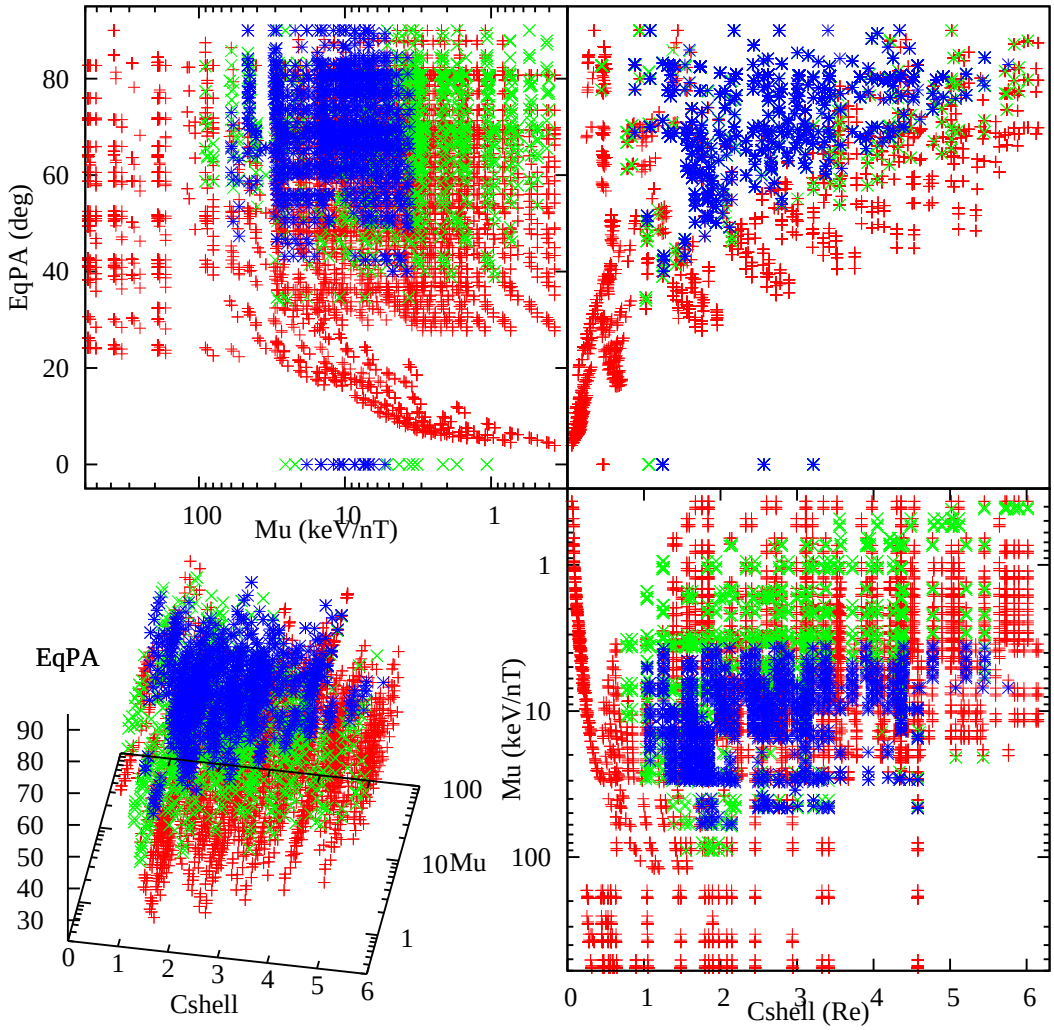

Figure 1. Electron trajectory phase space mapping in provisional cusp invariants: Red are chaotic, green quasi-trapped and blue trapped.

This preprint was prepared with AGU's LaTeX macros v4. File man05 formatted April 25, 2006.

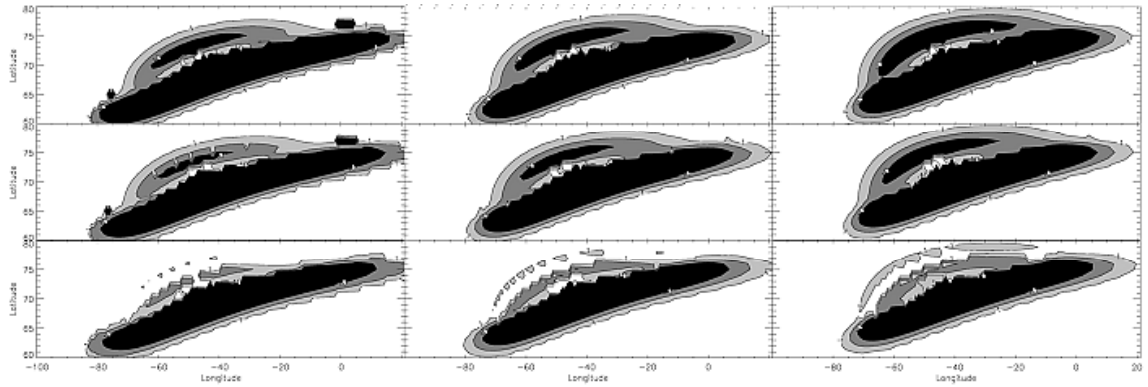

Figure 2. High latitude minima depth mapped to ionospheric latitude and longitude. Contours are at 1, 3, and 10 nT: columns at -3.7, +1.7, and +7.3 degrees dipole tilt toward sun; rows from top at 5, 3.3, 1.7 dynes pressure of solar wind.

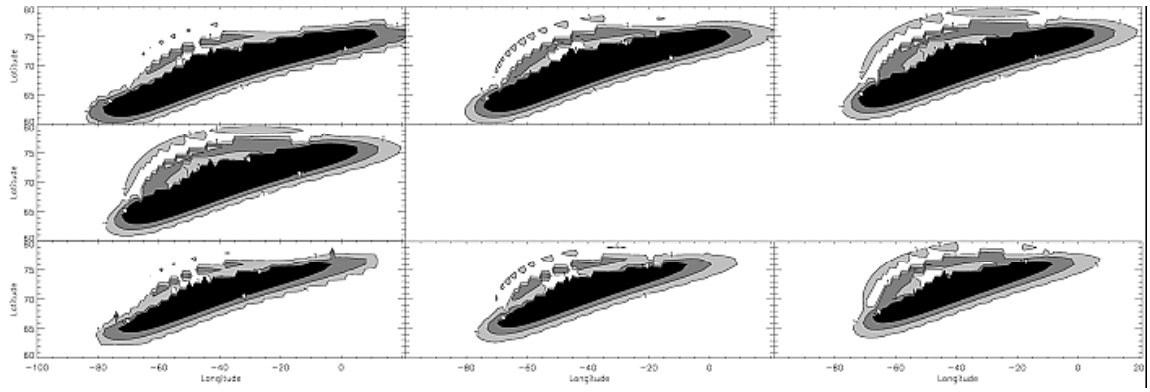

Figure 3. Minima contours with columns at -3.7, +1.7 and +7.3 degrees dipole tilt, rows from top at -50, -30, and -10 nT Dst.

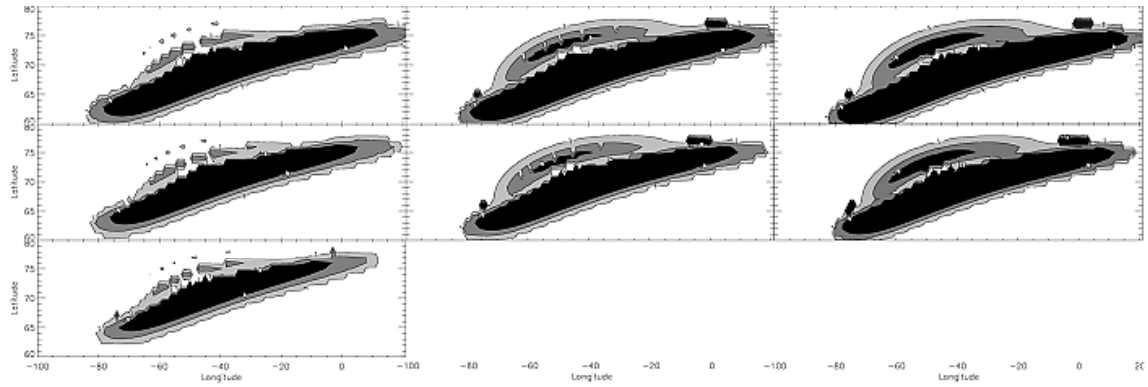

Figure 4. Minima contours with columns at 1.7, 3.3, and 5 dynes pressure solar wind, rows from top at -50, -30, -10 nT Dst

.